Zeitschrift: Schweizerische mineralogische und petrographische Mitteilungen = Bulletin suisse de minéralogie et pétrographie

Band: 82 (2002)

Heft: 2: Diagenesis and Low-Grade Metamorphism

Artikel: Mineral homogenization during low-temperature metamorphism. Part 1, Numerical models

Autor: Livi, Kenneth J.T. / Hinnov, Linda / Ferry, John M.

DOI: https://doi.org/10.5169/seals-62357

Nutzungsbedingungen

Die ETH-Bibliothek ist die Anbieterin der digitalisierten Zeitschriften auf E-Periodica. Sie besitzt keine Urheberrechte an den Zeitschriften und ist nicht verantwortlich für deren Inhalte. Die Rechte liegen in der Regel bei den Herausgebern beziehungsweise den externen Rechteinhabern. Das Veröffentlichen von Bildern in Print- und Online-Publikationen sowie auf Social Media-Kanälen oder Webseiten ist nur mit vorheriger Genehmigung der Rechteinhaber erlaubt. Mehr erfahren

Conditions d'utilisation

L'ETH Library est le fournisseur des revues numérisées. Elle ne détient aucun droit d'auteur sur les revues et n'est pas responsable de leur contenu. En règle générale, les droits sont détenus par les éditeurs ou les détenteurs de droits externes. La reproduction d'images dans des publications imprimées ou en ligne ainsi que sur des canaux de médias sociaux ou des sites web n'est autorisée qu'avec l'accord préalable des détenteurs des droits. En savoir plus

Terms of use

The ETH Library is the provider of the digitised journals. It does not own any copyrights to the journals and is not responsible for their content. The rights usually lie with the publishers or the external rights holders. Publishing images in print and online publications, as well as on social media channels or websites, is only permitted with the prior consent of the rights holders. Find out more

Download PDF: 15.01.2026

ETH-Bibliothek Zürich, E-Periodica, https://www.e-periodica.ch

SCHWEIZ. MINERAL. PETROGR. MITT. 82, 151–168, 2002

Mineral homogenization during low-temperature metamorphism Part 1: numerical models

by *Kenneth J.T. Livi*[1], *Linda Hinnov*[1], *John M. Ferry*[1], *David R. Veblen*[1] and *Martin Frey*[2] *(deceased)*

Abstract

It has been known that very low-grade metamorphic minerals will compositionally homogenize as time and temperature increase the metamorphic grade. To explain the natural data, three models of homogenization are presented and distinguished from each other on the basis of mineral zonation patterns and Fourier analysis of randomly measured compositional traverses. Numerical simulations of these models were made to determine the effects of relative differences in diffusivities in the solid and fluid on the homogenization process as recorded by Fourier analysis. Reaction-rate limited homogenization would produce flat intra-grain zonation patterns and equally reduces the variance of all frequencies in the Fourier spectrum. Diffusion-controlled homogenization of minerals in the presence of a grain boundary fluid that is considered an infinite, well-mixed reservoir would produce symmetric zonation patterns and reduces all frequencies in the Fourier spectrum equally. Diffusion-controlled homogenization in the presence of a grain boundary fluid of variable composition may create asymmetric zonation patterns and high-frequency suppression of the Fourier spectrum, if the diffusivity of the fluid is within a few orders of magnitude of that in the mineral.

An equilibrium domain within a rock may be considered a network of equilibrated mineral rims and grain boundary fluid that lace throughout the rock. The infinite–reservoir equilibration length scale, the distance over which the fluid and solid rim remain essentially constant in composition (which is a function of mineral size and the diffusivity ratio of mineral to fluid), is proposed as an adequate definition of equilibrium length scale.

Keywords: Diffusion, homogenization, low-temperature metamorphism, Fourier transforms.

Introduction

In studies of progressive low-temperature metamorphism, it is considered that sedimentary rocks with minerals in textural and chemical disequilibrium gradually approach equilibrium as temperature and/or time increase (e.g., PEACOR, 1992). This process manifests itself by (1) an overall increase in grain size, (2) migration of grain boundaries to develop simple grain shapes, (3) the removal of incompatible minerals, and (4) homogenization of mineral compositions. All of these processes have kinetic limits. Most investigations of the fourth process, compositional homogeneity, have concentrated on zonation patterns in coexisting minerals produced or modified by intra- and intergranular diffusion (e.g., LASAGA et al., 1977) and calculations of closure temperatures (e.g., DODSON, 1973). Yet, very little has been written on intergranular homogenization of minerals on the hand-sample scale and the information recorded in these variations until the last decade (BLACKBURN, 1968; VELDE et al., 1991; LIVI et al., 1992; LIVI, 1994; CHERNOFF and CARLSON, 1997). Homogenization in isotopic systems have been addressed by LASSEY and BLATTNER (1988), BICKLE (1992), DEPAOLO and GETTY (1996), and ABART and SPERB (1997).

Most recent studies considering the interplay of diffusion in the mineral volume and grain boundaries have centered on discontinuous reactions such as olivine + quartz = pyroxene (e.g., YUND 1997; FISLER et al., 1997; MILKE et al., 2001) or calcite + quartz = wollastonite (JOESTEN and

[1] The Morton K. Blaustein Department of Earth and Planetary Sciences, Johns Hopkins University, Baltimore, Maryland 21218, USA. <klivi@jhu.edu>

[2] Institute of Mineralogy and Petrography, Bernoullistrasse 30, CH-4056 Basel, Switzerland.

FISHER, 1988) where the reaction product growth rate is dependent upon the grain boundary diffusivity of the reactant species.

In this paper, and in a paper to follow, we have investigated intergranular and intragranular compositional heterogeneities and their progressive homogenization as a potential recorder of the kinetic controls of cation transport and exchange in rocks. Results from this study have a direct bearing on the estimate of the scale of equilibrium. The new approach we take is to consider the spatial distribution of variations in average mineral compositions within a rock. The quantification of the variance and frequency distributions of the data is achieved by Fourier analysis.

In part 1, we present numerical models that simulate different conditions of prograde homogenization of minerals reacting with a fluid with variable diffusivity. The emphasis of the present study is not only on intragranular zonation patterns, but on the spatial distribution of compositional fluctuations along linear traverses through rocks. These models demonstrate the importance of several parameters that can affect the rate and style of homogenization: reaction rate, the ratio of mineral to fluid diffusivities, modal abundances of minerals, the equilibrium distribution coefficient, and the total cation concentration in the fluid. In part 2, we present data from low temperature metamorphic shales from central Switzerland that demonstrate that homogenization does occur, and that techniques developed here can be used to determine the style of homogenization in natural samples.

Previous work and the definition of equilibrium domain

Previous mathematical treatments of exchange/diffusion processes consider relatively high-temperature conditions and assume that the system is in local equilibrium. They mainly deal with the effects of retrograde reactions and diffusive transport on the ability of a mineral (or minerals) to preserve a record of the peak metamorphic conditions or the cooling history of the rock. In contrast, our models simulate prograde reactions that alter a mechanical mixture of minerals with a range of composition to an equilibrium assemblage. Mineral exchange/diffusion calculations fall into two main categories: (1) exchange reactions between two phases in close proximity and of similar diffusivities (e.g., LASAGA et al., 1977; JIANG and LASAGA, 1990) and (2) reactions between a mineral and an infinite, well-mixed fluid (e.g., DODSON, 1973; GILETTI, 1986; EILER et al., 1992, and references within). In the following discussion, the former category will be referred to as "local reservoir equilibration" models, while the latter will be called the "infinite reservoir equilibration" models.

As applied to homogenization, the concept of local equilibrium would divide a rock into a number of *domains that contain homogeneous and equilibrated minerals*. With progressive metamorphic evolution (increased temperature and/or time), these domains may expand leading to the division of a system into fewer domains. The system, at any time, may be described as being in a state of mosaic equilibrium. Within each domain, the composition of a mineral depends upon that of the minerals next to it.

In our models, the rims of a mineral may equilibrate with a fluid in the grain boundary region. This fluid/grain boundary system is considered to be the main conduit for mass transport in the rock. At any given time, *the interior of the mineral may still be far from equilibrium with the fluid*. Thus, the definition of equilibrium domain would be considered a *network of equilibrated mineral rims and grain boundary fluid that lace throughout the rock*. The infinite reservoir equilibration model of diffusion maintains a homogeneous fluid that is in equilibrium with all rims. Thus the equilibrium scale for this model is the entire system of fluid and rims. In the local reservoir equilibration model, the fluid is allowed to vary in composition. Equilibrium lengths in the fluid (and thus the rims) would depend on the magnitude and wavelength of compositional variations.

In the discussion below, it will be demonstrated that a rock may be controlled by infinite reservoir equilibration conditions at small scales, while larger scales are controlled by local reservoir equilibration conditions; the relative size of each scale is related to the rate of homogenization by diffusion in the fluid versus that in the solid. Thus, a complete description of equilibrium requires knowledge of these scales. We present a concept that allows one to predict the relative local reservoir equilibration and infinite reservoir equilibration scales and the ratio of solid to fluid diffusivities from Fourier transforms of measured compositional traverse data.

In a recent paper, CHAKRABOTY and DOHMEN (2001) outlined a model investigating the influence of transport in solids and the intergranular medium and also the solubility of diffusing species in the intergranular medium. The model they present outlines important consequences of variable diffusivities in the fluid and solids and of the equilibrium distribution coefficient and is similar to our study. Their study supports the findings of

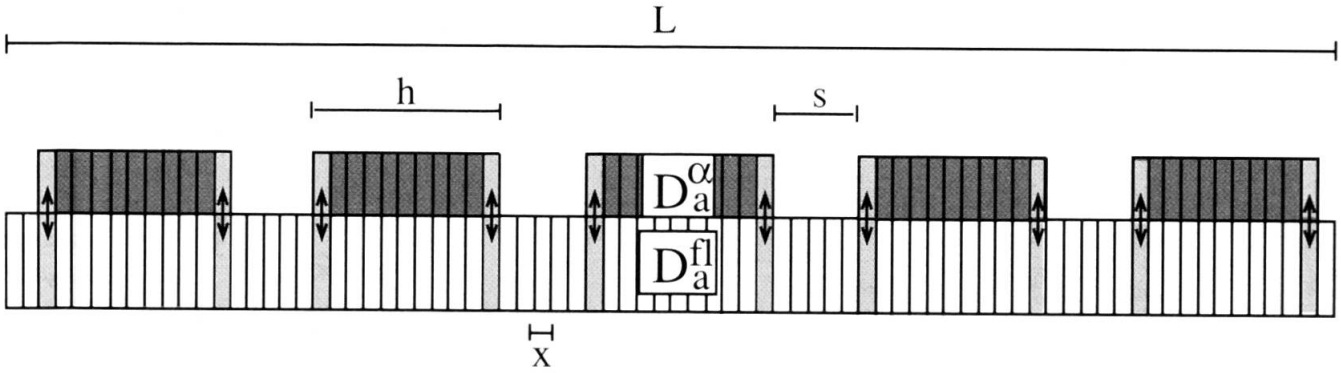

Fig. 1 Schematic representation of three numerical models. Dark shaded boxes represent solid mineral slabs. Open rectangles represent a continuous fluid within which the minerals are embedded. Light shaded rectangles are where exchange reactions take place between solid and fluid. RRL = reaction rate-limited model, ∞DL = infinite fluid diffusivity-limited model, FDL = finite fluid diffusivity-limited model.

LIVI (1994) and what we present here. The major difference in their approach is that their data is based on experiments involving a simple system with two solids and a gas medium, whereas, we consider an ensemble of minerals and investigate the evolution of compositional distributions by Fourier transforms.

Governing equations for homogenization

The basis for our homogenization models is illustrated in Fig. 1. The initial rock is composed of a hundred grains with pore space and grain boundaries between them. Exchange of the elements of interest, *a* and *b*, occurs in only one type of mineral, α, and if other minerals are present, they do not contain exchangeable *a* and *b*. The grains of α begin with a specified, arbitrary distribution of compositions. Each grain is initially homogeneous. Exchange of matter occurs through the *a*-*b* exchange reaction at mineral-fluid interfaces

$$a\alpha + b_{(aq)} \Leftrightarrow b\alpha + a_{(aq)} \qquad (1)$$

and is transported in a fluid through connected pores and grain boundaries. This is the only mechanism considered for mass transport between fluid and solid. Thus, the rate and extent of compositional changes in α are a function of the fluid composition at the solid-fluid interface. In the study of natural samples in part 2 of this paper, *a* and *b* are Fe^{2+} and Mg and the phase α is chlorite.

In natural systems, changes in composition of component *a* in the fluid (C_a^{fl})(moles/cm^3) over time (t) for any particular component are governed by the continuity equation:

$$\frac{\partial C_a^{fl}}{\partial t} = q + D_a^{fl}\frac{\partial^2 C_a^{fl}}{\partial x^2} \qquad (2)$$

which sums the contribution of matter produced/consumed from a mineral-fluid reaction (q), from one-dimensional diffusion where D_a^{fl} is the diffusion coefficient of *a* in the fluid for Fick's second law, and x is distance. Similarly, changes in the composition of a slab-shaped mineral (C_a^α) are governed by:

$$\frac{\partial C_a^\alpha}{\partial t} = q + D_a^\alpha\frac{\partial^2 C_a^\alpha}{\partial x^2} \qquad (3)$$

The quantity q, the surface exchange reaction, is related to the reaction rate (k_r) and the concentration of the reacting species by a rate law (see BERNER, 1981). Although the exact form is not important, a typical form may be:

$$q = \frac{dC_a^\alpha}{dt} = -k_r\left(\frac{C_a^\alpha - (C_a^\alpha)_e}{(C_a^\alpha)_e}\right)^z \qquad (4)$$

where $(C_a^\alpha)_e$ is the equilibrium value of *a* in α, and z is the order of the reaction. Distribution of *a* and *b* between solid and fluid is described by the equilibrium constant K_{eq},

$$K_{eq} = \frac{\left(C_b^{\alpha} / C_a^{\alpha}\right)}{\left(C_b^{fl} / C_a^{fl}\right)} \quad (5)$$

If we normalize the concentration of a in α in terms of number of moles (n_a^{α}) per total number of sites a may occupy per unit formula (s_t), we define X^{α} within a wafer of solid α:

$$X^{\alpha} = \frac{n_a^{\alpha}}{s_t} = \frac{n_a^{\alpha}}{n_a^{\alpha} + n_b^{\alpha}} \quad (6)$$

This is identical to parameters such as Fe/(Fe+Mg) in chlorite if no other atoms (i.e., Al) are exchanged in the octahedral sites. Compositional fluctuations in the fluid are related to the number of moles a in the fluid, n_a^{fl}, and the total chlorinity in moles (Cl_t),

$$X^{fl} = \frac{n_a^{fl}}{\frac{Cl_t}{2}} \quad (7)$$

for divalent cations. Here, Cl_t is a proxy for any monovalent complexing agent. With some manipulation, K_{eq} can be related to compositional fluctuations (see appendix for detailed derivation and solution of mass balance equations):

$$K_{eq} = \frac{\left(X^{\alpha} / (1 - X^{\alpha})\right)}{\left(X^{fl} / (1 - X^{fl})\right)} \quad (8)$$

Given a specified concentration of a in the mineral and fluid, K_{eq}, and Cl_t, the mass redistribution necessary for equilibrium at the mineral/fluid boundary can be calculated.

Three homogenization models

Three end-member homogenization processes are possible (ignoring advective mass transfer, recrystallization and growth of new minerals). (1) Reaction rate-limited homogenization occurs when diffusion is fast enough to homogenize any compositional perturbation in the solid or fluid created by reaction at the mineral-fluid interface. In this model, the entire homogeneous mineral progresses towards equilibrium in the presence of a fluid with constant composition at a given rate. This is a subset of the infinite reservoir equilibration model. Reaction rate laws may be of any kind. (2) Infinite fluid diffusivity-limited homogenization occurs when reaction rates are fast enough to maintain equilibrium at the mineral-fluid interface, and diffusion in the fluid is fast enough to maintain a homogeneous fluid. This is also a member of the infinite reservoir equilibration models. Changes in mineral composition are determined by the diffusivity of the elements in the solid. (3) Finite fluid diffusivity-limited homogenization occurs when fast reaction rates maintain equilibrium at the interface, and changes in the solid composition are related to both the mineral and fluid diffusivities. Local concentration gradients may build up in the fluid, depending upon the relative diffusivities of the fluid and solid. The finite fluid diffusivity-limited model can be described in terms of both the infinite reservoir equilibration model on small scales and the local reservoir equilibration model on larger scales.

DETAILS OF THE NUMERICAL MODELS

Computations assume an array of mineral slabs with unit widths and heights arranged so that their long axes are parallel to the fast diffusion direction (Fig. 1). Diffusion is assumed to occur only along this direction. The slabs are embedded in a continuous medium representing the fluid, where diffusion is also one-dimensional. Reactions only occur at the ends of the slabs. This seems justified in the case of some minerals such as chlorites since compositional gradients within their crystals occur mainly along the basal plane which is parallel to the long axis of the crystals (to be published in a future paper). Fluid is allowed to pass unreacted along their sides. This is necessary to maintain a continuous fluid medium and to prevent artificial gradients in fluid composition between slabs. In the one dimensional models considered, the solid fraction in the system is proportional to the sum of the lengths of the slabs divided by the total length of the fluid medium. Both the minerals and the fluid are subdivided into wafers with thicknesses x, so that $D/x^2 < 0.5$ for numerical stability (CARSLAW and JAEGER, 1959)(see appendix for details of diffusion calculations). Reactions at the mineral-fluid boundary are constrained by the equilibrium constant (Eq. 8). Although Fick's second law was derived for a single species, LASAGA et al. (1977) show that it is applicable to diffusion of two species in an otherwise fixed mineral structure where charge-balance requirements reduce the number of independent components to one. Similar simplifications may apply to the fluid which is considered to be a solution of H_2O and

single complexes of *a* and *b* (e.g., $FeCl_2$ and $MgCl_2$) and the concentration of the complexing agent is constant.

Numerical models followed three steps: (1) equilibration at solid-fluid boundary, (2) diffusion in the solid, and (3) diffusion in the fluid. However, assumptions for the reaction rate-limited model made it unnecessary to calculate steps 2 and 3, and step 3 is unnecessary for the infinite fluid diffusivity-limited model.

Reaction rate-limited model

The reaction rate-limited model is the simplest of the three models. Because the model assumes that diffusion in the solid and fluid is infinitely fast, both phases maintain homogeneous compositions and the fluid is held at a constant composition. Each slab begins with an arbitrarily assigned homogeneous composition. We normalize the slab compositions (X^α) to have a zero mean value and assume that $X^\alpha = 0$ is the equilibrium value for all slabs. As reaction of the slabs with the fluid progresses, each mineral slab approaches zero *X*-value in composition at a rate prescribed by the rate law.

Infinite fluid diffusivity-limited model

The infinite fluid diffusivity-limited model assumes that reaction rates are fast enough to maintain equilibrium at the mineral-fluid boundary during one time step, the fluid has an infinite diffusivity, and the solid a finite diffusivity. Each slab begins with an arbitrarily assigned composition, X_0^α, with a zero mean for the entire slab population. The infinite diffusivity of the fluid is represented by considering a fluid with everywhere constant composition, $X_0^{fl} = 0$. Therefore, boundary conditions for each slab of length *h* are at $t > 0$:

$$x = x_o: X^\alpha = 0,$$
$$x = x_o + h: X^\alpha = 0,$$

(i.e., the rims are equilibrated to zero), and at $t = 0$ the slab is originally homogeneous:

$$0 < x < x_o + h: X^\alpha = X_0^\alpha.$$

Diffusion in the mineral slab proceeds independently of its neighbors. Matter diffuses within the mineral because of compositional gradients near the slab boundaries imposed by equilibration with the fluid. Diffusion profiles are thus created in the slabs. Average slab compositions $\bar{X}^\alpha$ were calculated at designated time steps. This model is a numerical analog of the approximate analytical solution of SHEWMON (1963, pages 16–18) derived for slabs of length *h* evolving by diffusion:

$$\frac{\bar{X}^\alpha}{X_0^\alpha} = \frac{8}{\pi^2}\exp\left(-\frac{\pi^2 D_a^\alpha t}{h^2}\right) \quad (9)$$

This equation is valid for:

$$\bar{X}^\alpha / X_0^\alpha \leq 0.8.$$

Finite fluid diffusivity-limited model

The principle assumption in this model is that reaction rates are fast enough to maintain equilibrium at the mineral-fluid boundary during each time step. The boundary conditions during the portion of the calculation in which diffusion occurs in the solid are (1) a homogeneous starting composition at t = 0, and (2) zero diffusion flux across the solid-fluid boundary. These constraints guarantee mass balance and decouple diffusion in the solid from diffusion in the fluid allowing exchange of matter *only by reaction* and not by diffusion. The boundary conditions computing diffusion in the fluid are zero flux at the extreme boundaries (total length, *L*, of fluid medium is the sum of lengths, *h*, of all solid slabs plus the spaces, *s*, between slabs), with either a homogeneous starting composition $X_0^{fl} = \bar{X}^\alpha$ or with variable linear composition gradients. Linear gradients are calculated by establishing equilibrium near the end of each mineral and specifying linear compositional profiles in regions between minerals. As calculations progress, the boundary compositions for each slab depend upon the ability of the fluid to homogenize local compositional perturbations created by fluid/mineral reactions. If the diffusivity in the solid is great, diffusion maintains a homogeneous composition in each mineral slab as the fluid composition evolves. Under these conditions, this model simulates reaction rate-limited homogenization with an evolving fluid. If diffusivity in the solid is not fast enough to homogenize the slab, diffusion profiles will develop in the slab. Similarly, if the diffusivity of the fluid is great, diffusion can homogenize the entire fluid reservoir.

VALIDITY OF MODEL ASSUMPTIONS

There are several important assumptions in these models. The first assumption is that the fluid medium can be modeled as one continuous medium with constant *D*. This assumption does not strictly apply to nature. However, if deviations from an average diffusivity in the fluid are randomly dis-

tributed in a rock, they should not effect homogenization in a systematic fashion. We assume sampling traverses are longer than the scale of any fluctuation in D^{fl}. The second assumption, that mineral grains are one size with diffusion in one direction (parallel to slab length), has already been addressed. A third assumption deals with the compositional simplicity of our model – both in the solid and fluid. Although samples with only one Fe-Mg mineral occur in nature, real metamorphic fluids are not as simple as in our models. This is an oversimplification, the effects of which are unknown. Finally, we assume that mineral growth and dissolution do not occur. We have ignored these phenomena for the sake of simplicity. The addition of material to a mineral slab would increase the time needed for the entire mineral to homogenize, while dissolution would shorten it. This is modeled in the calculations that consider variations in the length and spacing of slabs. However, these calculations are static (i.e., they do not change during the homogenization process). Exactly how dynamic slab sizes would affect homogenization needs further study.

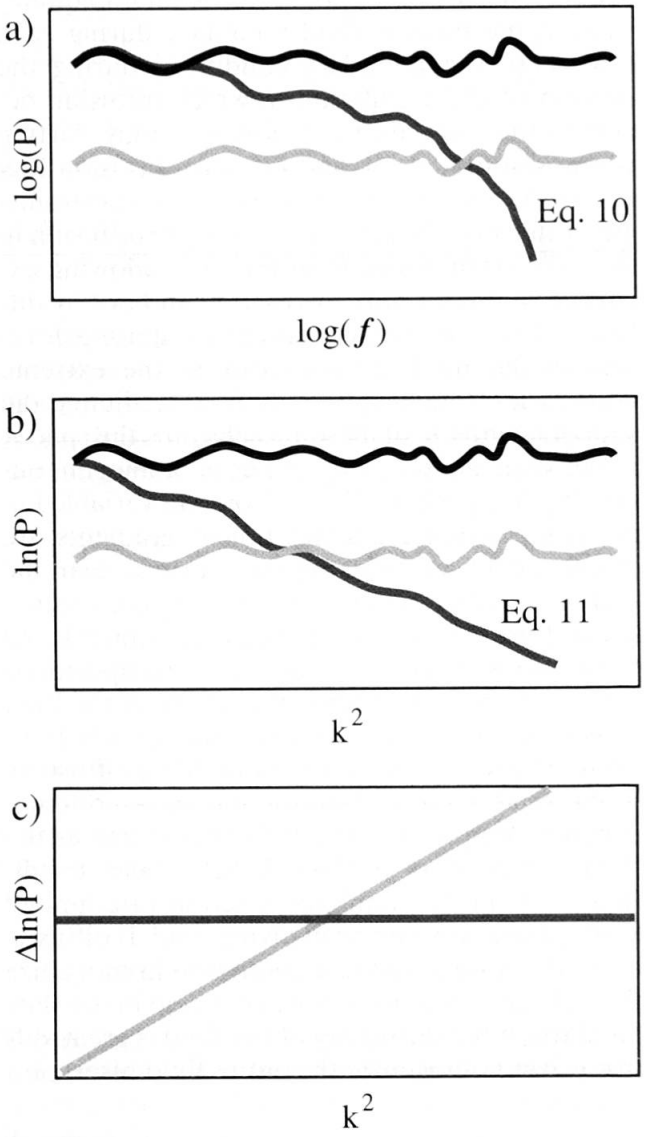

Fig. 2 Schematic illustration of the effects of diffusion in a continuous medium on Fourier spectra. (a) The black line is the original spectrum, the medium gray line is after diffusion has taken place (Eq. 10), and the light gray line is after a process not dependent upon frequency has modified the original data. (b) The plot of the natural log of power versus wavenumber squared for the same spectra as in 6a. (c) Smoothing of curves in 6b by plotting $\Delta\ln(P)$ versus k^2.

Fourier analysis

The numerical simulations presented here generate both zonation patterns internal to the mineral slabs and average slab compositions along a traverse. The average compositions contain information on whether neighboring slabs have influenced each other's compositions as homogenization progresses. This "memory" of neighboring compositions can be detected by Fourier transform methods (see Appendix 2 for computational details). A freeware program can be obtained from the URL listed in Appendix 2.

The Fourier transform is a mathematical tool used to analyze the second order moment statistics (variance) of stationary, Gaussian processes as a function of frequency (MARPLE, 1987). Through the method known as the separation of variables, Fourier transforms have also been used to model diffusion processes (SHEWMON, 1963; CRANK, 1975). We use the Fourier transform to estimate the distribution of variance, or the "power" (P), of the *average slab composition data* and model results as a function of spatial frequency (f) along linear arrays of model slabs or sampled transects in natural samples. Fourier analysis describes a data series as a combination of sine and cosine functions with variable frequencies and amplitudes. In this context, low frequencies represent long wavelength (distance) variations, and high frequencies are short wavelength variations. Power at a particular frequency is proportional to the square of the amplitude, and measures the variance contained at that frequency. Thus, noisy, random, or inhomogeneous data will contain power at all frequencies, while clean, identical or homogeneous data will contain no power at frequencies $f \neq 0$. Since the Fourier transform can separate out the variance contained in different frequencies, it is ideal for determining the effects of processes that influence low and high-frequency data differentially. Diffusion is one such process.

Three-dimensional diffusion in an isotropic continuous medium will dampen compositional

fluctuations according to the equation (BATCHELOR, 1953, p. 92–93):

$$P_t = P_0 e^{-2Dtk^2} \quad (10)$$

where P_t is the spectral power (Fourier transform) of the fluctuations at time t, P_0 is the Fourier transform of the original fluctuations, and k is the wavenumber ($k = 2\pi f$). Equation 10 is also a valid approximation to one-dimensional transforms of three-dimensional diffusion when k is small (BATCHELOR, 1953). This equation dictates that the power of the transform decays with k^2. Therefore, higher frequencies will be suppressed more quickly than lower frequencies. Frequency suppression is related to neighboring compositional fluctuations influencing each other – local short-wavelength and high compositional gradients are reduced more rapidly than long-wavelength and low compositional gradients. The expression of Eq. 10 is illustrated in the medium gray curve on the log(P)–log(f) (P–f) diagram in Fig. 2a, where the original spectrum is the black line. As the frequency increases, the reduction of power becomes greater and the curve drops to the right. However, if a process is not dependent upon frequency, then the spectrum will drop in power *without a change in slope* (light gray line in Fig. 2a).

If we take the natural logarithm of Eq. 10

$$\ln(P_t) = \ln(P_0) - 2Dtk^2 \quad (11)$$

the function is now linear if plotted on a ln(P)–k^2 diagram (P–k) (medium gray line in Fig. 2b). The y-intercept marks the power of the original spectrum, and the slope is a function of Dt. In general, the slope is modified by a function related to the geometry of the system – in the case of an isotropic continuous medium, it has a value of 2. If homogenization is not a function of frequency, the slope of the original spectrum does not change, and there is simply a drop in power for all frequencies (light gray line Fig. 2b). By plotting the difference between the natural logarithm of the original and homogenized spectra $\Delta\ln(P) = \ln(P_0)-\ln(P_t)$ against k^2, fluctuations in the curves are smoothed (Δ–k diagrams; Fig. 2c). P–f, P–k, and Δ–k diagrams will be used to illustrate how homogenization proceeds in numerical models and natural data (part 2). Applying these plotting methods to numerical results, the average composition of each mineral slab becomes one datum in a spatial series. In generating the Fourier series, only the solid compositions were considered; the fluid compositions were ignored. Results from numerical models will differ from Eqs. 10 and 11 since the medium analyzed is not continuous but a series of discrete slabs embedded in a fluid.

Results of numerical models

REACTION RATE-LIMITED

A zero-order rate law ($z = 0$ in Eq. 4) was chosen in the simulation of linear reaction-rate limited homogenization. A portion of the original data is presented in Fig. 3a. After homogenization proceeded up to a reaction extent of $-\Delta tk = 0.2$ in Eq. 4, the slab compositions changed but retained flat intramineral composition patterns (Fig. 3b). This is required for infinitely fast diffusion in the solid. The P–f diagram for the calculation is presented in Fig. 3c. Two features are important to note: (1) the original slope of the spectrum did not change as homogenization proceeded, and (2) the original frequency distribution (peaks and valleys) changed but there was no systematic suppression of high frequencies. These features are to be expected from a process that is not spatially dependent. All mineral slabs reacted with a fluid with the same constant composition, and each mineral slab reacted at a designated rate. There is a change in frequency distribution which can be seen in minor changes in the shape of the curve. This derives from the fact that slab compositions slow down as they approach equilibrium and ceased changing when they reach equilibrium (zero), and slab compositions far from equilibrium change faster. However, since high and low compositions are spatially randomly distributed, they will not cause a frequency dependent shift in the Fourier spectrum.

INFINITE FLUID DIFFUSIVITY-LIMITED

As in the reaction rate-limited model, the P–f diagram for the infinite fluid diffusivity-limited model shows that there is an overall reduction of power with no systematic suppression of frequencies (Fig. 4b). The original frequency distribution is preserved as homogenization progresses. This is similar to reaction rate-limited homogenization when the rate law is a function of composition in the solid (i.e., $z > 0$ in Eq. 4). The difference between the reaction rate-limited and infinite fluid diffusivity-limited models is in the intramineral zonation patterns. Figure 4a shows that all minerals exhibit symmetric zonation patterns with identical rim compositions. The rate of composition change can be approximated by Shewmon's equation (Eq. 9), which works as well when the stand-

ard deviation of the population is substituted for composition.

FINITE FLUID DIFFUSIVITY-LIMITED

The finite fluid diffusivity-limited results are divided into sections dealing with the effects of the main variables. The starting fluid composition for all computations presented is that of steady-state. Results vary depending upon the starting compositions for calculations using phases of similar diffusivities. However, differences in results for calculations when phases have very different diffusivities were determined to be insignificant, as long as the number of time steps was about 10^4 or greater.

Finite fluid diffusivity-limited: Effects of relative solid and fluid diffusivities

Results from six calculations with diffusivity differences of up to five orders are presented in *P–f*

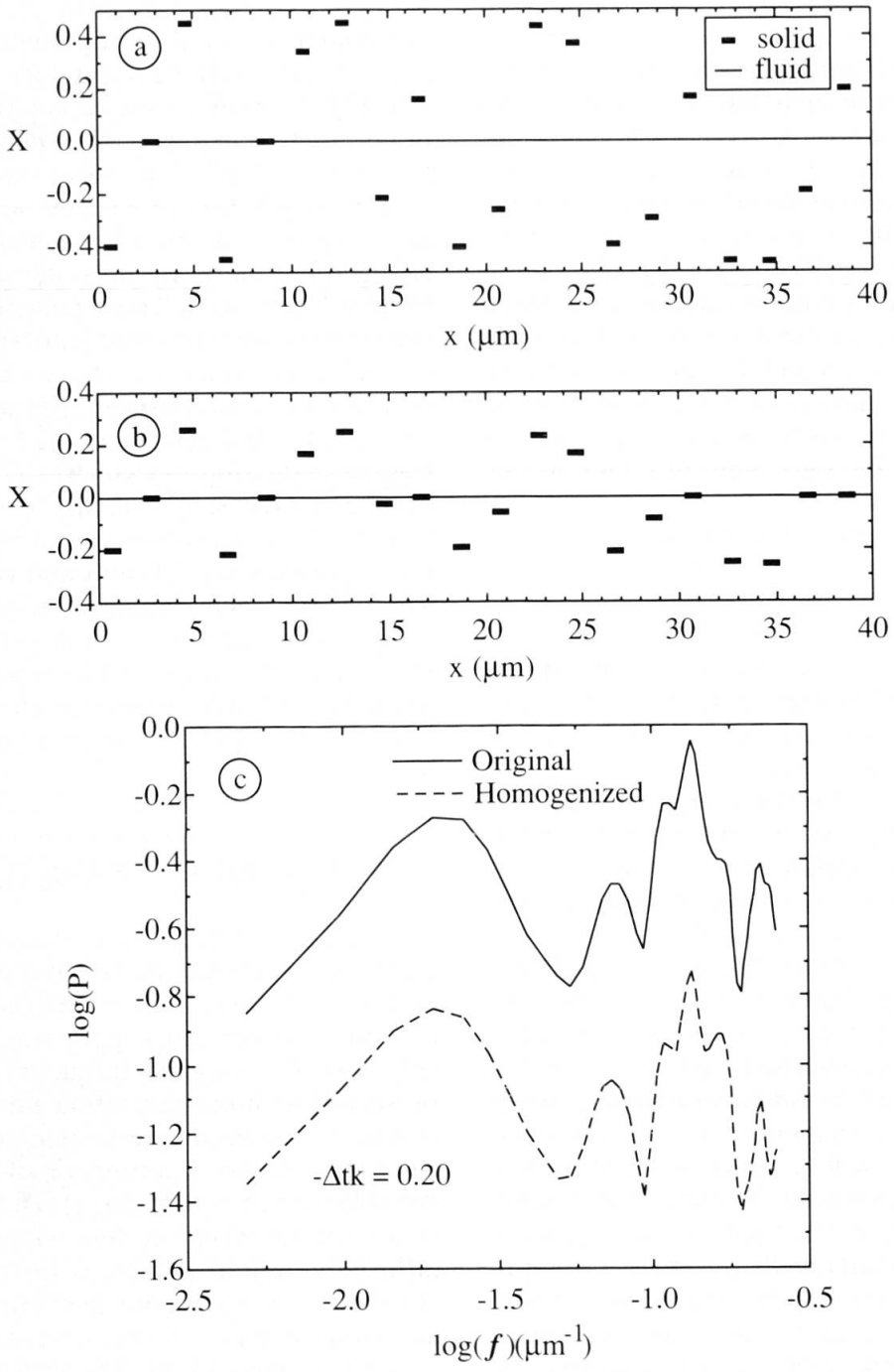

Fig. 3 Results of reaction rate-limited numerical modeling. (a) Original mineral zonation patterns for the first twenty slabs. (b) Mineral zonation patterns for the first twenty slabs after homogenization. (c) Fourier spectra.

diagrams in Figs. 5a–f and in the Δ–k diagrams in Figs. 6a, b. Each calculation was run for the same number of time steps. In Fig. 5a, where there is a five-order of magnitude difference in fluid and solid diffusivities, the reduction of power is nearly evenly distributed over all frequencies, and the original shape of the spectrum is preserved. This is similar to the infinite fluid diffusivity-limited results in Fig. 4a. As the diffusivity contrast decreases, the intensity of high-frequency suppression increases (Figs. 5b–d). Theoretically, the homogenization curves in Figs. 5d–f should drop to infinitely small values. However, the precision of the calculations did not permit the resolution of fluctuation differences less than ~10^{-5}. Therefore, when fluctuation differences reach log(P) values of –5, the calculation error creates the artificial plateaus seen in the high-frequency portions of Figs. 5d–f.

When the value of D^{α} is 10^{-4} μm^2/s (10^{-13} m^2/s) or greater (Figs. 5e and f), the diffusion process is fast enough to nearly homogenize a 1-μm slab within one time step. Therefore, Figs. 5e and f represent a modified version of the reaction rate–limited model where, instead of a fixed fluid composition, the fluid evolves with time. Figure 6a combines the six calculations on a Δ–k plot. As the difference between solid and fluid diffusivities increases, the degree of homogenization (height of curve on Δ–k plot) decreases (for a fixed fluid diffusivity). The maximum height on this curve is limited by the precision of the calculations. The change in style is particularly evident in the blowup of Fig. 6a in Fig. 6b. Notice that calculation "A" reaches the same degree of homogeneity in the high-frequency region (log(f) > 1) as "B", but attains greater homogeneity in the low-frequency region. This is because the two calculations have the same mineral diffusivity (which will control the ultimate degree of homogenization), but faster fluid diffusivity in "A" than in "B".

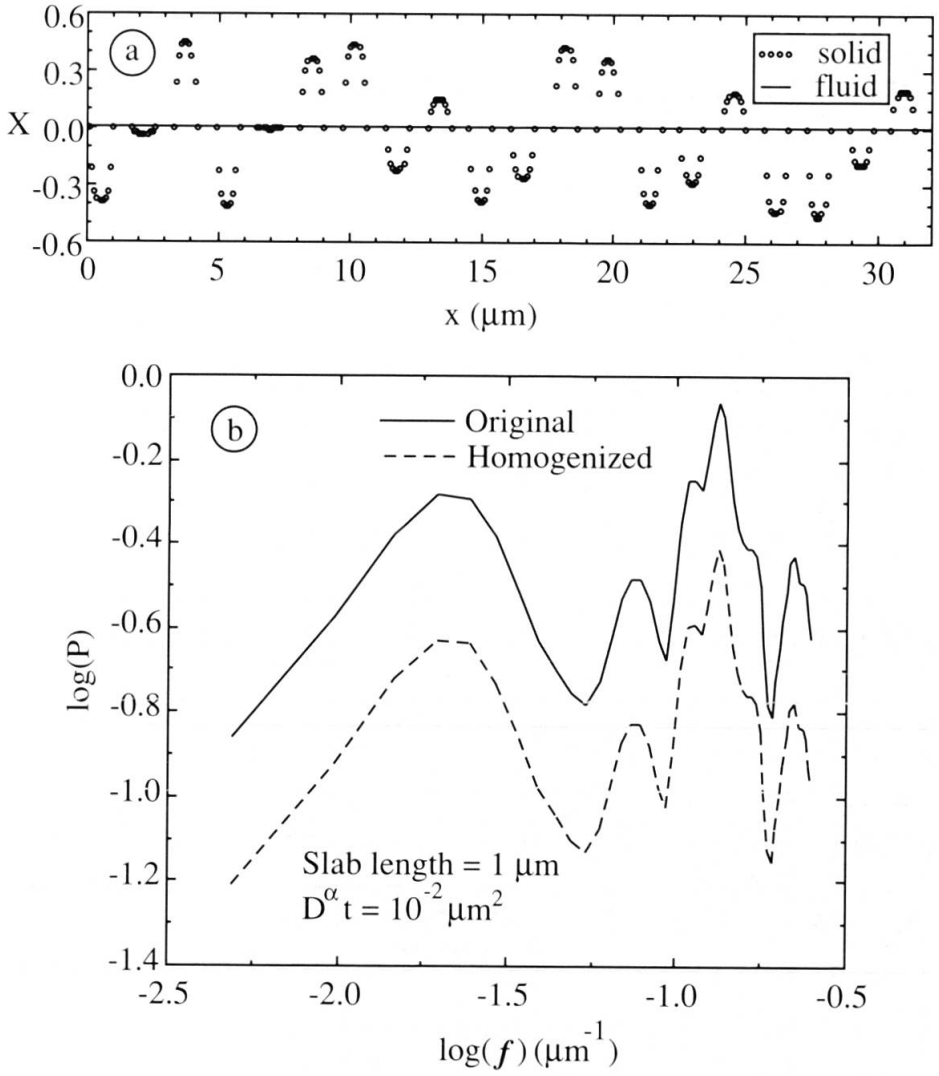

Fig. 4 Results of infinite fluid diffusivity-limited numerical modeling. (a) Mineral zonation patterns for the first twenty slabs after homogenization. (b) Fourier spectra.

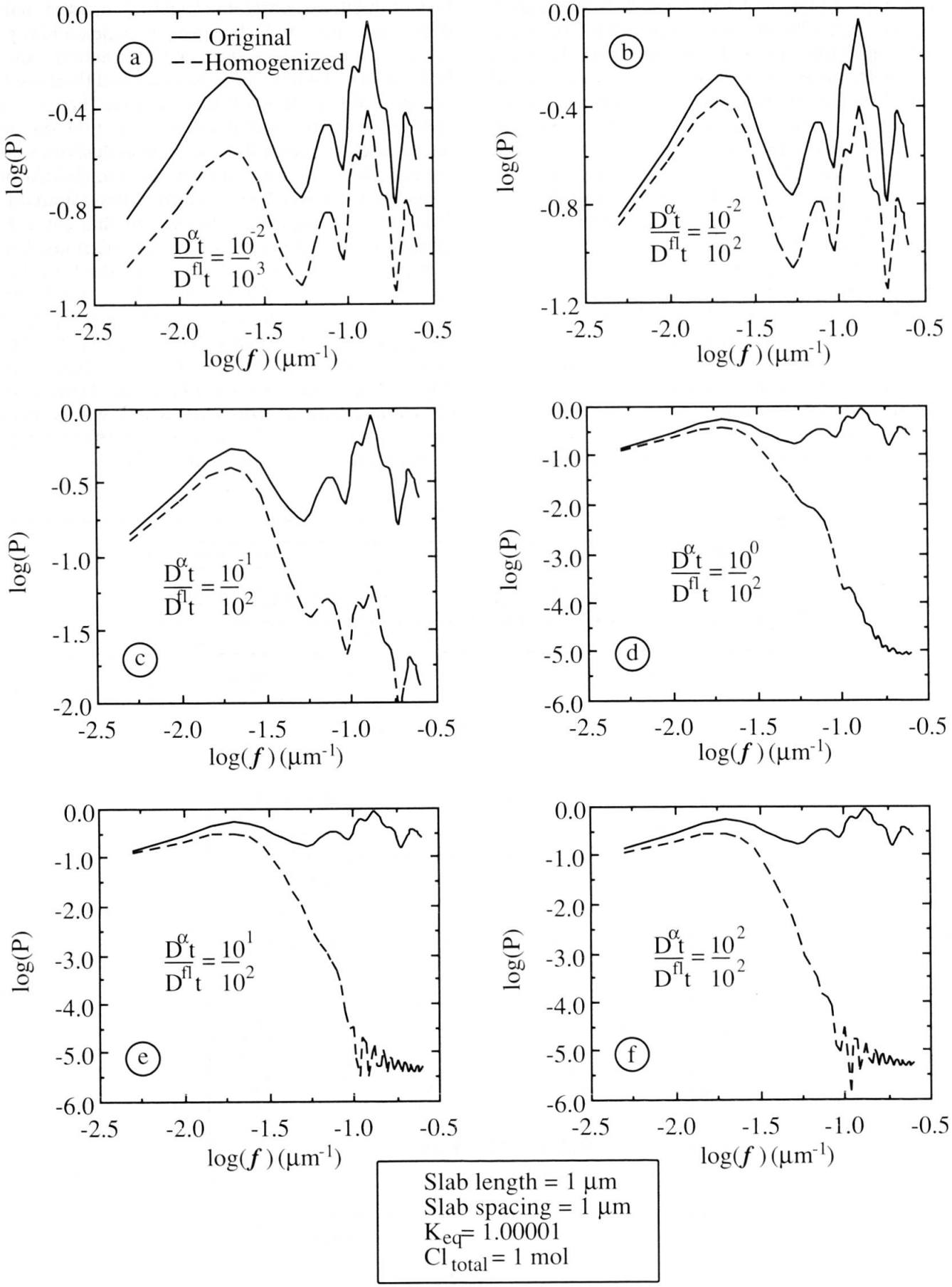

Fig. 5 Fourier spectra of six finite fluid diffusivity-limited numerical modeling calculation results with different mineral and fluid diffusivities.

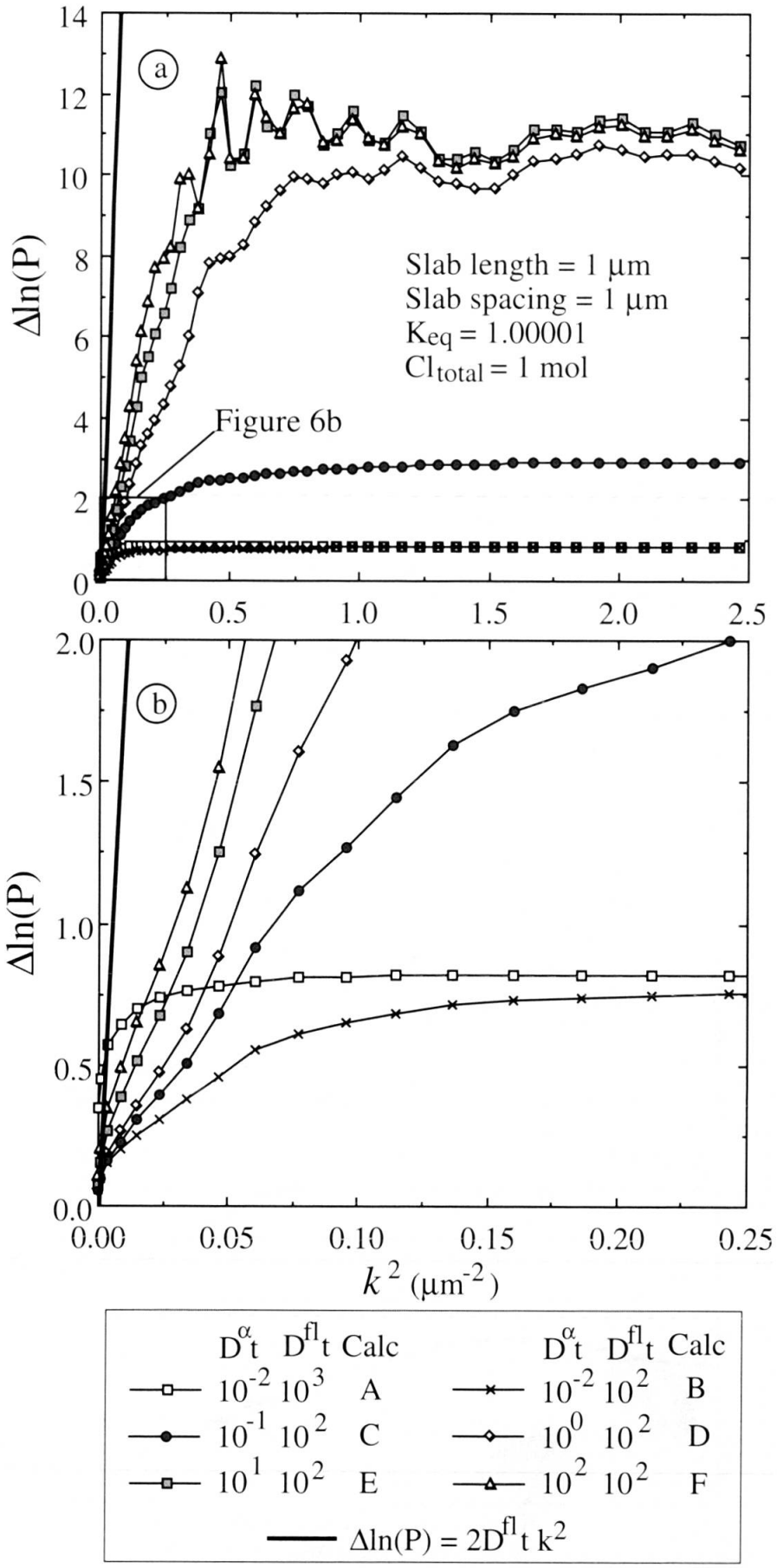

Fig. 6 Δ–k plots of the six finite fluid diffusivity-limited numerical modeling calculations shown in Fig. 5. Letters a through f correspond to calculations in Figs. 5a through 5f.

In each spectrum, the low-frequency portion reflects the character of the evolving fluid that is influenced by the exchange of matter with the minerals. Thus, as frequency decreases or sampling length-scale increases, mineral compositions will exhibit increasingly more local reservoir equilibration characteristics. Note, however, that the low-frequency portion of calculation "F" ($D^{\alpha}/D^{fl} = 1$) approaches but does not have the same slope as what would be expected for an isotropic medium (solid line), and as the difference in diffusivities increases, the slopes decrease. The relationship between the slope (β) and the ratio of the diffusivities in the calculation (with $h = 1$ μm, s = 1 μm, $K_{eq} = 1.0001$, $Cl_t = 1$ mol) is related empirically by

$$\beta = 33 + 3 \ln(D^{\alpha}/D^{fl}). \quad (12)$$

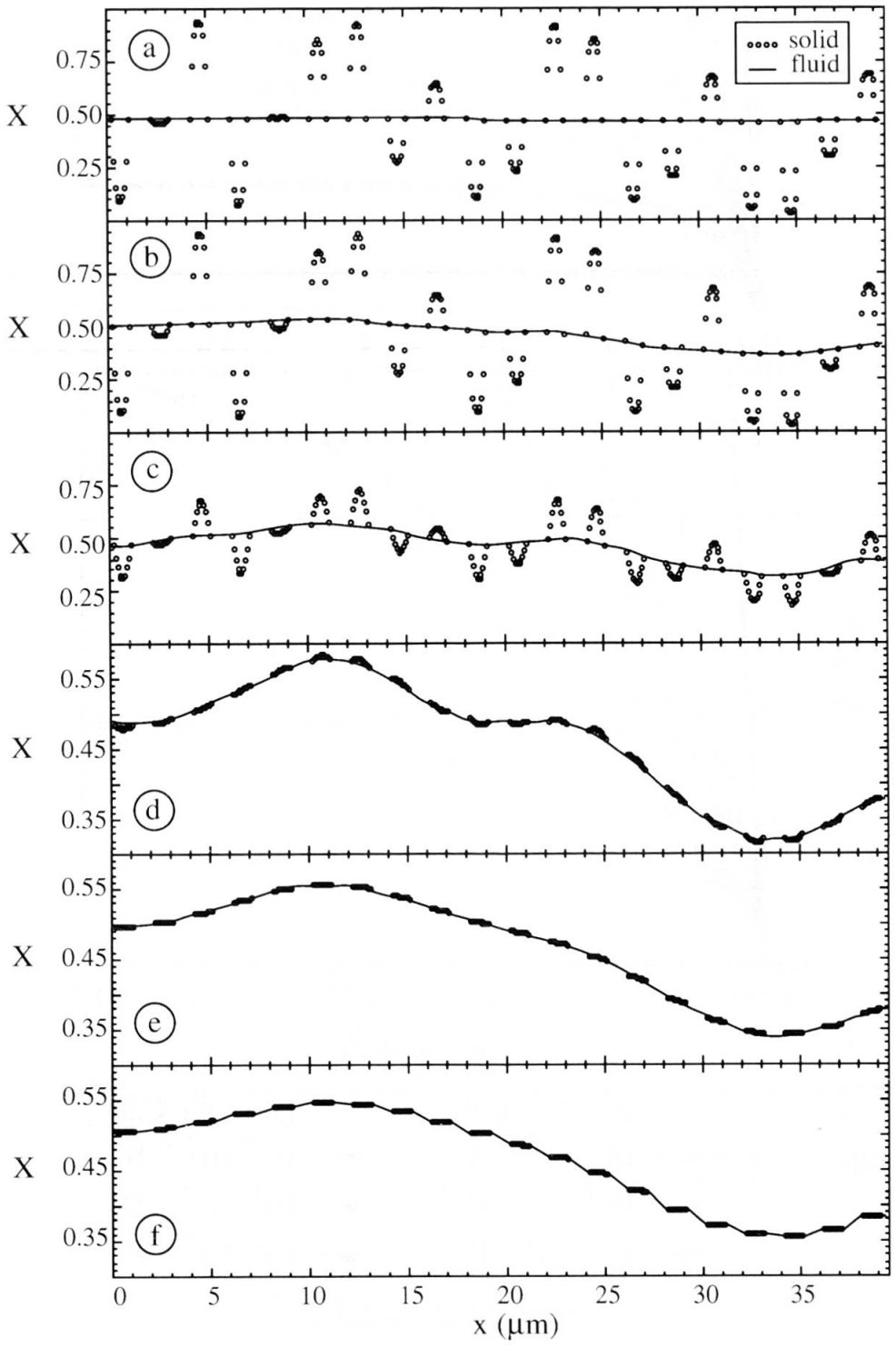

Fig. 7 Mineral zonation patterns of six finite fluid diffusivity-limited numerical modeling calculation results. Letters a through f correspond to calculations in Figs. 5a through 5f.

In contrast, as frequency increases or sampling length scale decreases, mineral compositions will increasingly reflect infinite reservoir equilibration characteristics. Using the square root of the power of the high-frequency portions of the spectra as estimates of the standard deviation in Eq. 9 gave $D^{\alpha}t = 2.2 \times 10^{-2}$ μm² for simulations "A" and "B" and $D^{\alpha}t = 1.1 \times 10^{-1}$ μm² for simulation "C", which agrees well with the expected values of 10^{-2} and 10^{-1} μm², respectively. Therefore, the calculations "A", "B", and "C" are consistent with the analytical expression of SHEWMON (1963). $D^{\alpha}t$ for simulation "D" was calculated at 4.9×10^{-1} μm² which is half of what it should be. This is because the error in the calculations is greater than the compositional differences at high-frequencies in this simulation.

The zonation patterns of the first twenty slabs and the local fluid for each of the six calculations are given in Figs. 7a–7f. The patterns for the solids in $D^{\alpha}t = 10^{1}$ (Fig. 7e) and $D^{\alpha}t = 10^{2}$ (Fig. 7f) are nearly flat because of their high diffusivity. Note that the fluid is not homogeneous in these cases. This is because the rate at which matter is exchanged by reaction (and the diffusion transport of matter in the solid to the interface) keeps pace with diffusion in the fluid. Zonation of solids in Figs. 7a and b are relatively symmetric and the fluid is nearly homogeneous. Comparing these results (7a and b) with that of the infinite fluid diffu-

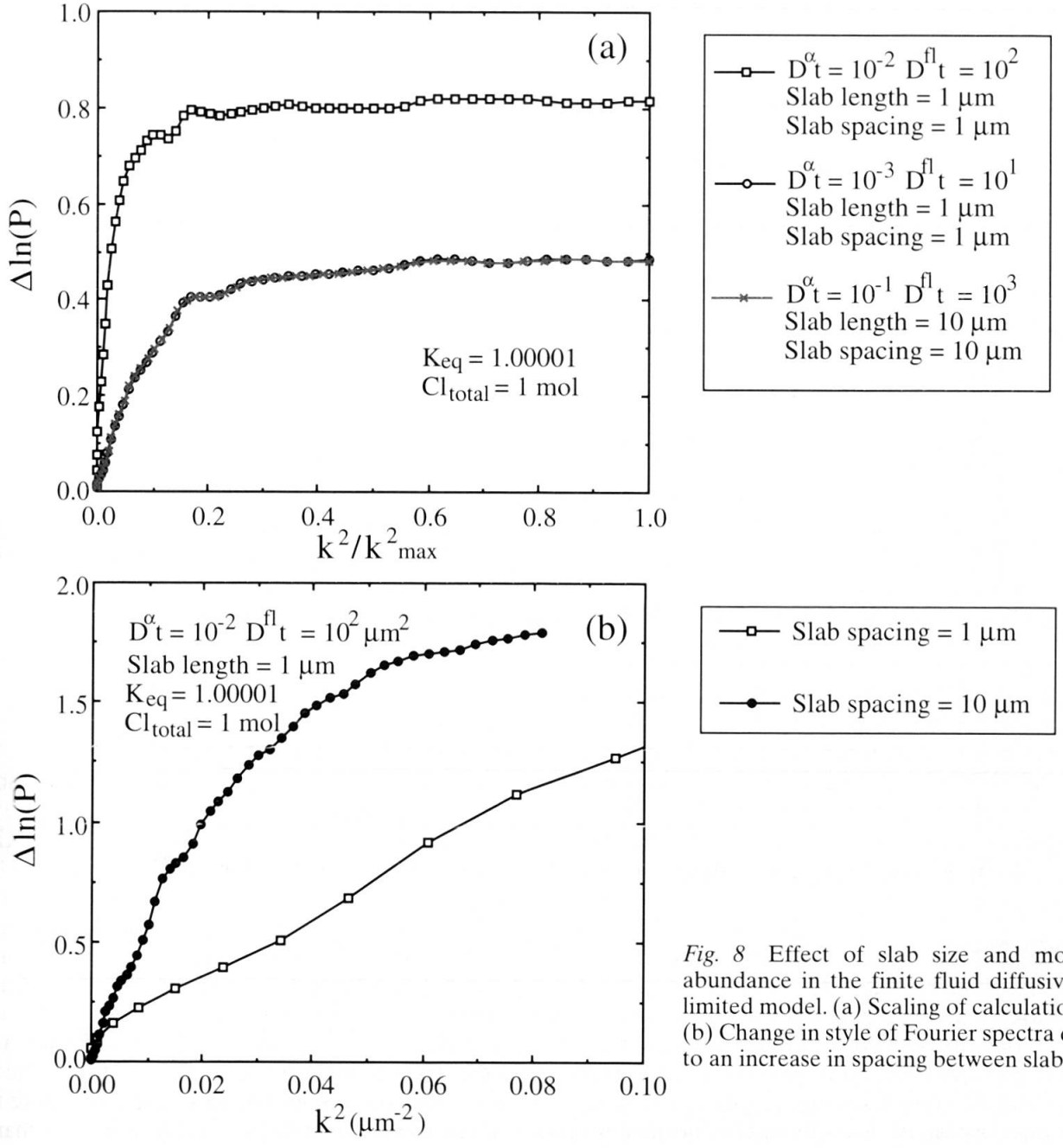

Fig. 8 Effect of slab size and modal abundance in the finite fluid diffusivity-limited model. (a) Scaling of calculations. (b) Change in style of Fourier spectra due to an increase in spacing between slabs.

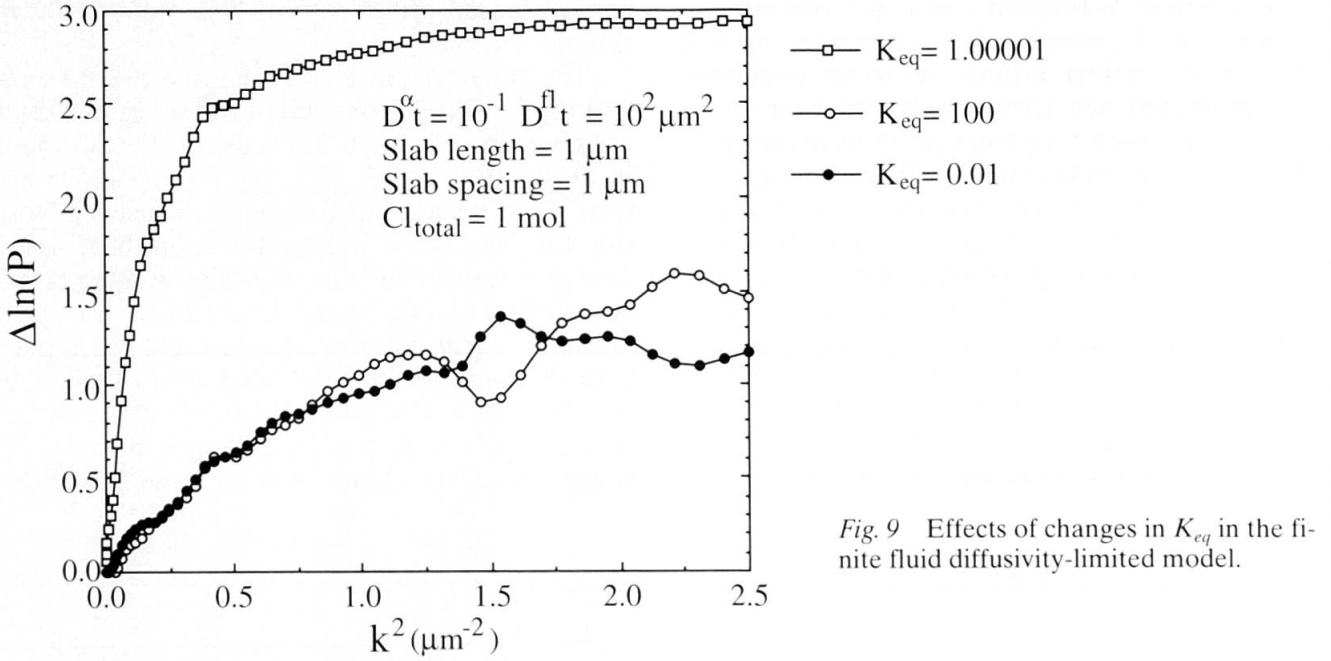

Fig. 9 Effects of changes in K_{eq} in the finite fluid diffusivity-limited model.

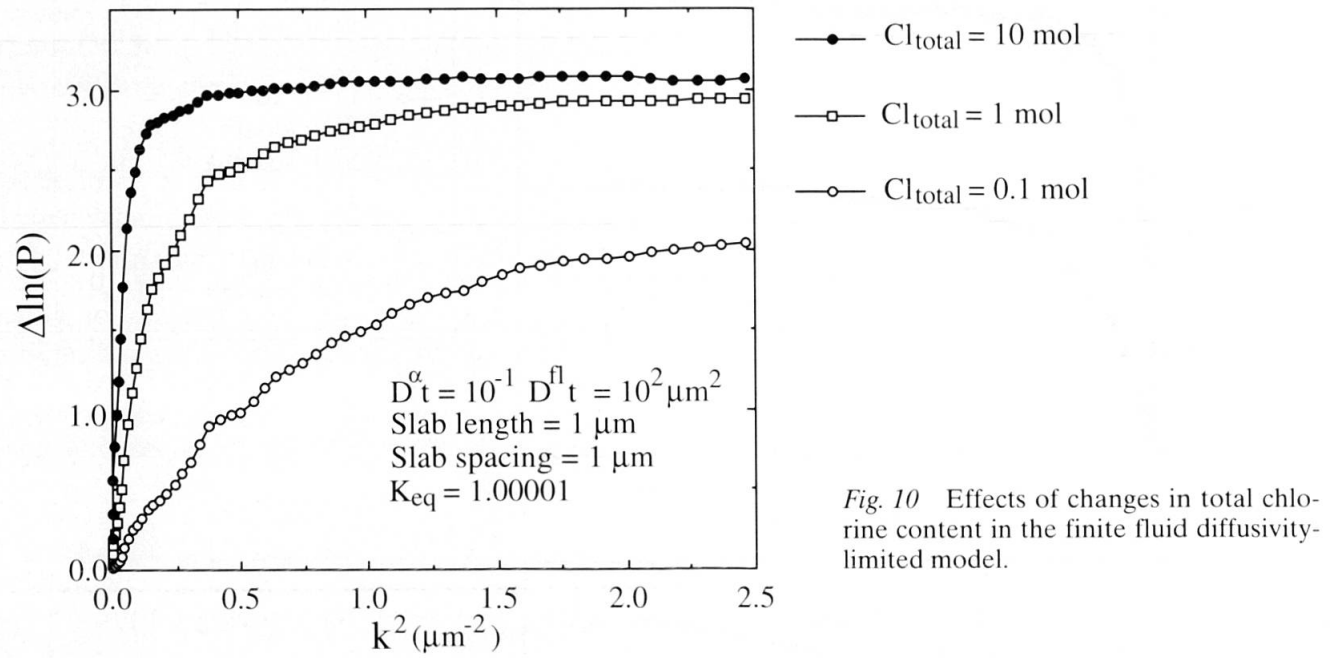

Fig. 10 Effects of changes in total chlorine content in the finite fluid diffusivity-limited model.

sivity-limited model (Fig. 4) show that they are nearly identical. Zonation of solids in Figs. 7c, d and e exhibit both symmetric and asymmetric patterns and the fluid has an intermediate degree of homogenization. Only in these cases are asymmetric compositional zonation patterns produced in minerals.

Finite fluid diffusivity-limited: Effects of slab size and modal abundance

Increase in slab lengths (h) effectively increases the amount of material that has to be homogenized, and therefore, the time to reach a certain degree of homogenization is longer. The style of homogenization is also affected by the spacing (s) of slabs. Hence, to completely describe a system, both length and spacing need to be specified. Both of these parameters are related the modal abundance of phase α.

Figure 8a demonstrates how the calculations may be scaled by plotting $\Delta\ln(P)$ versus k^2/k^2_{max}, which effectively normalizes all wavenumbers to the sampling rate. Increasing both the length (h) and spacing (s) of the model by an order of magnitude requires an increase of two orders of magnitude in the diffusivities of both solid and fluid to maintain the same Δ–k profile for the same total time. The modal abundance of minerals in the system has not changed in this case. Also note that the ratio of diffusivities is not required to change.

By comparison, an increase in s with constant h reduces the modal abundance of α and the amount of mineral that must be homogenized. This has the effect of increasing the rate of homogenization (Fig. 8b). Only the low-frequency portion of the 1-μm spacing calculation is presented, because of the differences in scale between the two calculations. The increased spacing of slabs decreases the effects of nearest neighbors on each other, making the Δ–k curve flatten more quickly than in the closer-spaced calculation. Increasing h while keeping s constant increases the modal abundance of the mineral and slows homogenization. Effects of changing spacings become less pronounced as the difference in diffusivities becomes greater. In fact, when the infinite fluid diffusivity-limited model applies, the spacing of α has no effect on the style or rate of homogenization. Only the length of the slab does.

Finite fluid diffusivity-limited: Effects of K_{eq}

Figure 9 clearly shows a reduction in the degree of homogenization when K_{eq} differs from 1. Interestingly, the response to either a two-order increase or decrease in K_{eq} is an equivalent reduction in homogenization. This is because K_{eq} determines the magnitude of f in both the fluid and solid (Eq. 8), and either a low or high value of K_{eq} means that one of the phases will be inefficient at exchanging the two components. Unlike slab spacing, the style and degree of homogenization will be sensitive to K_{eq} regardless of the ratio of solid and fluid diffusivities.

Finite fluid diffusivity-limited: Effects of total chlorinity

The total amount of chlorine (or the complexing ligand) in the fluid also has an effect on the rate and style of homogenization (Fig. 10). Increases in chlorinity accelerate homogenization and reduces nearest-neighbor effects. This is due to an increase in mass transfer for a given reaction interval (more of a and b in the fluid requires greater changes in solid compositions during boundary equilibrations). This increases the rate of change in mineral composition at the mineral-fluid interface. This, in turn, causes steeper composition gradients and increases diffusion rates within the mineral. Decreasing chlorinity has the opposite effect.

Discussion

Through numerical models, we have demonstrated that different types of homogenization processes produce different shapes of Fourier spectra and mineral zonation patterns. The simulations show that infinite fluid diffusivity-limited homogenization will lower the power in all frequencies. In contrast, finite fluid diffusivity-limited homogenization affects mainly the high frequencies. Fourier transforms of the model data clearly show this effect. Other factors such as slab size and spacing, total chlorinity, and the equilibrium constant have the effect of accelerating or decelerating the rate of slab homogenization. An order of magnitude increase in the chlorinity of the fluid is equivalent to two orders of magnitude change of K_{eq} from unity, but is less effective at homogenizing the slabs than a change of an order of magnitude difference in solid/fluid diffusivities. These parameters can be grouped into two categories: (1) transport variables such as the diffusivities of the solid and fluid, and (2) gradient variables such as K_{eq}, total chlorinity, and slab size/spacing that change the chemical potential gradients.

In nature, the combination of factors contributing to homogenization will be complex and vary spatially. Exact prediction of the rates of homogenization of any particular rock would require knowledge of all the features outlined above and how they vary within the rock. This is obviously impossible. The best one can hope for is to lump all of these variables together into an effective time-integrated spatially-averaged exchange/transport parameter. However, the use of Fourier transforms of mineral compositional transects within a rock would still give information about the response of homogenization to local equilibrium. This investigation is presented in part 2 of this paper where natural chlorite compositions were gathered along linear traverses and analyzed by Fourier methods. The models presented here are the groundwork for gaining further insight on the complex process of equilibrating sediments during low-temperature metamorphism and other geological processes involving diffusion homogenization.

In addition to the Fourier analyses, our models show that the Shewmon equation is applicable to homogenization of minerals. This may prove to be a simple tool for estimating the parameters involved in the homogenization process. Its application to natural data is presented in part 2. Combining these data with detailed chemical analyses of zonation patterns in single crystals should reveal evidence for local changes in the fluid composition (asymmetric zonation) or a homogeneous local fluid composition (symmetric zonation).

Acknowledgements

This paper evolved from a suggestion from A. Lasaga, many fruitful discussions with O. Phillips on the mathe-

matics of diffusion, and talks with G. Fisher on diffusion in geologic processes. We thank J. Brady, C. de Capitani, R. Abart, and R. Ferreiro-Mählmann for their insightful reviews that greatly improved the manuscript. Lastly, we dedicate this paper to Martin Frey. His pioneering work in the Alps showed that systematic and careful study could coax the secrets out of reticent low-grade rocks.

References

ABART, R. and SPERB, R. (1997): Grain-scale stable isotope disequilibrium during fluid-rock interaction. 1: series approximations for advective-dispersive transport and first-order kinetic mineral-fluid exchange. Am. J. Sci. 297, 679–706.

BATCHELOR, G.K. (1953): The theory of homogeneous turbulence. Cambridge University Press, Cambridge, UK. pp. 92–93.

BERNER, R.A. (1981): Kinetics of weathering and diagenesis. In: LASAGA, A.C. and KIRKPATRICK, R.J. (eds): Kinetics of Geochemical Processes. Rev. Mineral. 8, 111–130.

BICKLE M.J. (1992): Transport mechanisms by fluid-flow in metamorphic rocks: oxygen and strontium decoupling in the Trois Seigneurs Massif – a consequence of kinetic dispersion? Am. J. Sci. 292, 289–316.

BLACKBURN, W.H. (1968): The spatial extent of chemical equilibrium in some high-grade metamorphic rocks from the Grenville of Southeastern Ontario. Contrib. Mineral. Petrol. 19, 72–92.

BRADY, J. (1983): Intergranular diffusion in metamorphic rocks. Am. J. Sci. 283A, 181–200.

CARSLAW, H.S. and JAEGER, J.C. (1959): Conduction of Heat in Solids. Claredon Press, Oxford. 510 pp.

CHAKRABORTY, S. and DOHMEN, R. (2001) Some aspects of the role of intergranular fluids in the compositional evolution of metamorphic rocks. Proc. Indian Acad. Sci. 110, 293–303.

CHERNOFF, C.B. and CARLSON, W.D. (1997): Disequilibrium for Ca during growth of pelitic garnet. J. Metamorphic Geol. 15, 421–438.

CRANK, J. (1975): The mathematics of diffusion. Oxford University Press, Oxford. 414 pp.

DEPAOLO, D.J. and GETTY, S.R. (1996): Models of isotopic exchange in reactive fluid-rock systems: implications for geochronology in metamorphic rocks. Geochim. Cosmochim. Acta 60, 3933–3947.

DODSON, M.H. (1973): Closure temperature in cooling geochronological and petrologic systems. Contrib. Mineral. Petrol. 40, 259–274.

EILER, J.M., BAUMGARTNER, L.P. and VALLEY, J.W. (1992): Intercrystalline stable isotope diffusion: A fast grain boundary model. Contrib. Mineral. Petrol. 112, 543–557.

FISLER, D.K., MACKWELL, S.J. and PETSCH, S. (1997): Grain boundary diffusion in enstatite. Phys. Chem. Minerals 24, 264–273.

FREER, R. (1981): Diffusion in silicate minerals and glasses: A data digest and guide to the literature. Contrib. Mineral. Petrol. 76, 440–454.

GILETTI, B.J. (1986): Diffusion effects on oxygen isotope temperatures of slowly cooled igneous and metamorphic rocks. Earth Planet. Sci. Lett. 77, 218–228.

HARRIS, F.J. (1978): On the use of windows for harmonic analysis with the discrete Fourier transform. Proceedings of the IEEE 66, 51–83.

JENKINS, G.M. and WATTS, D.G. (1968): Spectral analysis and its applications. Holden-Day, San Francisco. 254 pp.

JOESTEN, R. and FISHER, G. (1988): Kinetics of diffusion-controlled mineral growth in the Christmas Mountains (Texas) contact aureole. Geol. Soc. Am. Bull. 100, 714–732.

JIANG, J. and LASAGA, A.C. (1990): The effect of post-growth thermal events on growth-zoned garnet: Implications for metamorphic P-T history calculations. Contrib. Mineral. Petrol. 105, 454–459.

LASAGA, A.C., RICHARDSON, S.M. and HOLLAND, H.D. (1977): The mathematics of cation diffusion and exchange under metamorphic conditions. In: SAXENA S.K. and BHATTACHARJI, S. (eds): Energetics of Geological Processes. Springer-Verlag, New York. pp. 353–388

LASSEY, K.R. and BLATTNER, P. (1989): Kinetically-controlled oxygen isotope exchange between fluid and rock in one-dimensional advective flow. Geochim. Cosmochim. Acta 52, 2169–2175.

LIVI, K.J.T. (1994): Low-temperature metamorphism of Liassic clastic sediments from the Central Switzerland. Unpublished Ph.D. thesis, Johns Hopkins University, 323 pp.

LIVI, K.J.T., FERRY, J.M. and VEBLEN, D.R. (1992): Mineral homogenization during low-temperature metamorphism of shale. IGCP Conference on Low-Temperature Metamorphism, Davis, California, September, 1992.

MARPLE, S.L.J. (1987): Digital Spectral Analysis with Applications. Prentice-Hall, Englewood Cliffs, New Jersey. 492 pp.

MILKE, R., WIEDENBECK, M. and HEINRICH, W. (2001): Grain boundary diffusion of Si, Mg, and O in enstatite reaction rims: A SIMS study using isotopically doped reactants. Contrib. Mineral. Petrol. 142, 15–26.

PAILLARD, D., LABEYRIE, L. and YIOU, P. (1996): Macintosh program performs time-series analysis. EOS Trans. 77, p. 379.

PEACOR, D.R. (1992): Diagenesis and low-grade metamorphism of shales and slates. In: BUSECK, P.R. (ed.): Minerals and Reactions at the Atomic Scale: Transmission Electron Microscopy .Rev. Mineral. 27, 335–380.

SHEWMON, P.G. (1963): Diffusion in Solids. McGraw-Hill, New York. 203 pp.

VELDE, B., El MOUTAOUOKKIL, N. and IIJIMA, A. (1991): Compositional homogeneity in low-temperature chlorites. Contrib. Mineral. Petrol. 107, 21–26.

YUND, R.A. (1997): Rates of grain boundary diffusion through enstatite and forsterite reaction rims. Contrib. Mineral. Petrol. 126, 224–236.

Manuscript received December 10, 2001; revision accepted July 22, 2002.
Editorial handling: R. Ferreiro Mählmann

Appendix 1

Calculation of changes in composition due to diffusion followed the explicit central difference method of CARSLAW and JAEGER (1959), so that for one time step (t)

$$\Delta X_{i,t+1} = D * \frac{\left(X_{i-1,t} - 2 * X_{i,t} + X_{i+1,t}\right)}{x^2} \quad \text{(A1)}$$

where X_i is the magnitude of the fluctuation in the ith wafer of length x. For the boundaries of slabs and fluid media

$$\Delta X_{i,t+1} = D * \frac{\left(2 * X_{i\pm1,t} - 2 * X_{i,t}\right)}{x^2} \quad \text{(A2).}$$

This creates a zero-flux boundary for both the minerals and the extreme ends of the fluid reservoir.

If concentration is scaled on a molar basis, and n_a^α is the number of moles of a per mole of α in Eq. A3, s_t is the total number of sites that a and b enter per formula unit, n_a^{fl} is the number of moles of a per mole of fluid, Cl_t is the total number of moles of chlorine per mole of fluid, $\bar{V}^\alpha$ is the molar volume of mineral α, and $\bar{V}^{fl}$ is the molar volume of fluid, then we have

$$n_a^\alpha = C_a^\alpha \bar{V}^\alpha \quad \text{(A3)}$$
$$n_a^{fl} = C_a^{fl} \bar{V}^{fl} \quad \text{(A4)}$$
$$n_a^\alpha + n_b^\alpha = s_t, \text{ and} \quad \text{(A5)}$$
$$Cl_t = \nu\,(n_a^{fl} + n_b^{fl}) \quad \text{(A6)}$$

where $\nu = 2$ for divalent cations. The dimensionless compositional fluctuations (X) for the fluid and solid are:

$$X^{fl} = \frac{\nu n_a^{fl}}{Cl_t} \quad \text{(A7)}$$

and

$$X^\alpha = \frac{n_a^\alpha}{s_t} \quad \text{(A8).}$$

To recast the equilibrium constant equation

$$K_{eq} = \frac{\left(C_b^\alpha / C_a^\alpha\right)}{\left(C_b^{fl} / C_a^{fl}\right)} \quad \text{(A9)}$$

in terms of fluctuations, we substitute Eqs. A3 through A8 into Eq. A9 and obtain

$$K_{eq} = \frac{\left(X^\alpha / \left(1 - X^\alpha\right)\right)}{\left(X^{fl} / \left(1 - X^{fl}\right)\right)} \quad \text{(A10).}$$

Reaction at the mineral-fluid boundary redistributes matter, so that mass is conserved and A10 is satisfied. Given that n_α^t is the total number of moles of a in the bordering mineral and fluid wafers and each wafer having volumes V_s and V_{fl}, respectively, and,

$$n_a^t = C_a^\alpha V_s + C_a^{fl} V_{fl}$$

$$n_a^t = \frac{X^\alpha V_s}{\bar{V}^\alpha} + \frac{\frac{1}{2} Cl_t X^{fl} V_{fl}}{\bar{V}^{fl}} = aX^\alpha + bX^{fl},$$

$$a = \frac{V_s}{\bar{V}^\alpha} \quad \text{(A11)}$$

$$b = \frac{Cl_t V_{fl}}{\nu \bar{V}^{fl}} \quad \text{(A12)}$$

and,

$$X^\alpha = \frac{n_a^t - bX^{fl}}{a} \quad \text{(A13).}$$

Plugging Eq. A13 into A10 and solving for X^{fl}, we obtain the quadratic equation:

$$\left(K_{eq}\, b/a - b/a\right)(X^{fl})^2 +$$

$$\left(K_{eq} - K_{eq}\, n_a^t/a + n_a^t/a + b/a\right)(X^{fl}) + \left(-n_a^t/a\right) = 0 \quad \text{(A14)}$$

$$X^{fl} = \frac{-B - \sqrt{B^2 - 4AC}}{2A} \quad \text{(A15)}$$

where:

$$A = b/a\left(K_{eq} - 1\right) \quad \text{(A16)}$$

$$B = K_{eq}\left(1 - K_{eq}\right) n_a^t/a + b/a \quad \text{(A17)}$$

$$C = n_a^t/a \quad \text{(A18).}$$

Appendix 2

For discrete, finite processes, P may be calculated using the Blackman-Tukey spectral estimator:

$$P(f) = \phi \sum_{m=-\Lambda}^{+\Lambda} w_m r_m \exp[-i2\pi f m\phi] \qquad (A19)$$

where ϕ is the sampling interval of the process (spatial in our case), r_m is the autocorrelation estimate of the N-sampled process at lag m, f is frequency defined over the range $-(2\phi)^{-1} \leq f \leq +(2\phi)^{-1}$, w_m is the Hann lag window described in HARRIS (1978), and Λ is the total number of autocorrelation lags, where $\Lambda = 0.3N$. For real processes, $P(-f) = P(f)$, and so we restrict our calculation to $0 \leq f \leq +(2\phi)^{-1}$. We apply a slight modification of this estimator in order to render the estimated values proportional to spectral power (variance), as opposed to spectral power density (dependent on ϕ), namely we calculate $(N\phi)^{-1} P(f)$ (see MARPLE, 1987, p. 151, for details) where N is the number of points in the series. Finally, we accommodate the large dynamic range of $P(f)$ by displaying the results in $\log(P)$–$\log(f)$ space.

The error of $P(f)$ depends and the spectral properties of w_m. The degrees of freedom ν of $P(f)$ depend on w_m; for the Hann window, $\nu = 8N/(3\Lambda)$, where N is the number of process values (JENKINS and WATTS, 1968). It has been shown that $P(f)$ follows a χ^2_ν-distribution with ν degrees of freedom; the $100(1-\alpha)\%$ confidence interval for $P(f)$ is thus:

$$[\nu P(f)/\chi^2_\nu(1-a/2), \nu P(f)/\chi^2_\nu(\alpha/2)]$$

Figure A1 illustrates the procedure applied to a discrete, second order autoregressive process, i.e., a process containing a predictive measure of nonrandomness. The estimated power spectrum reveals that the low frequencies contain the majority of the process variance, with peak power occurring in a band of frequencies centered at $f' = 0.125$ (i.e., $\log(f') = -0.9$). This indicates the presence of a characteristic wavelength near $\phi\,(f')^{-1} = 8$; this is visible in the original process (Fig. A1a). The absence of high frequencies is reflected in a rapid drop-off of power for $f > 0.2$ ($\log(f) > -0.7$) in Fig. A1b. In log-log space, the 95% confidence interval is constant with respect to f. The Blackman-Tukey estimator can be performed using the freeware ANALYSERIES (PAILLARD et al., 1996) available at the website www.agu.org/eos_elec/96097e.html.

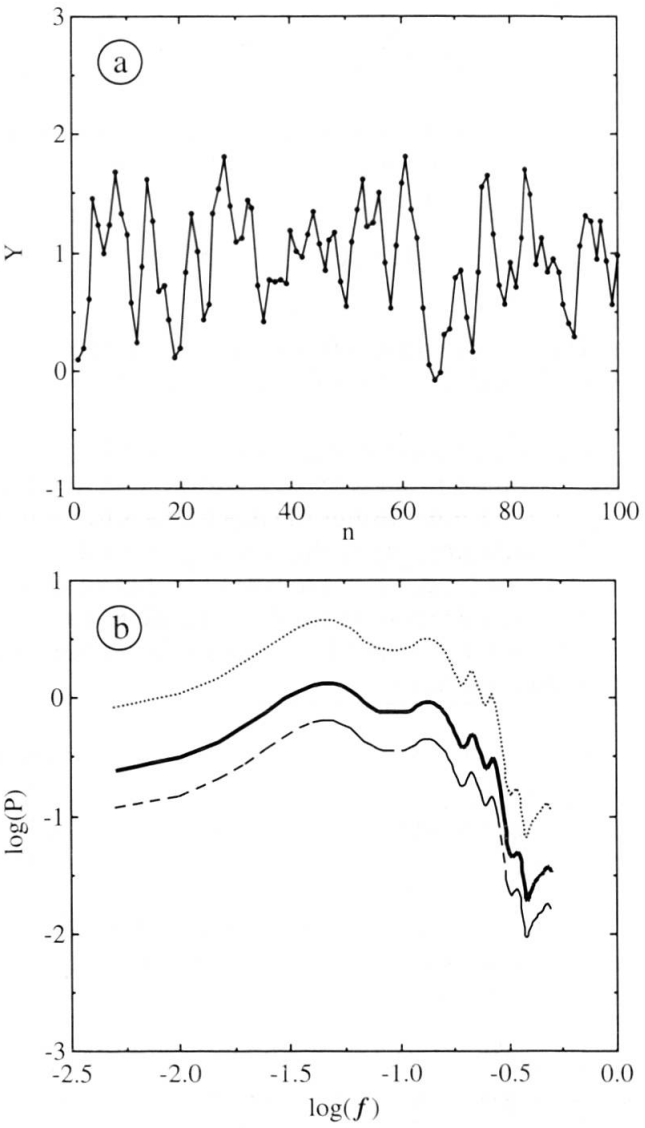

Fig. A1 An illustration of Fourier analysis of a process containing a degree of non-randomness. (a) Fluctuations (Y) of a hypothetical process along a series of n measurements. Notice the presence of a characteristic wavelength of about $n = 8$. (b) Fourier spectrum in log(power)-log(frequency) space of data in A1a. The non randomness of the process reduces variance at high frequencies which is reflected by the rapid drop of power at $\log(f)$ values greater than –0.7.